TOWARDS AN OBJECTIVE PERFORMANCE MEASURE OF SPACEBORNE WIND SENSORS: ERS TEST CASE

M. Portabella and A. Stoffelen

Royal Dutch Meteorological Institute (KNMI), Postbus 201, 3730 AE De Bilt, The Netherlands
Emails: portabel@knmi.nl; stoffele@knmi.nl

ABSTRACT

In order to look for a generic scatterometer inversion method, the ERS inversion is revisited in this paper. First, the use of measurement noise information, which includes a realistic geophysical noise term, is tested. It turns out that the shape of the solution surface is more important than the noise information for inversion. Such shape has to be symmetric or circular as a function of wind direction in order to produce realistic and accurate wind direction distributions. A method, which looks for the measurement space transformation that produces such symmetric properties is then presented. In contrast with some previous work performed along these lines, the proposed method is generic. The results show indeed improved wind direction skill compared to the more traditional (measurement-noise normalization) inversion for ERS.

1 INTRODUCTION

Spaceborne wind observations have proven important for a wide variety of applications, including nowcasting, short-range forecasting and mesoscale numerical weather prediction (NWP) data assimilation. However, because of the different spatial and temporal sampling characteristics as well as the different error statistics of the various spaceborne systems, the comparison among the different wind sources is not trivial. In addition, the error analysis for wind data derived from spaceborne sensors requires special care due to non-linearities and ambiguities in the geophysical model functions (GMF) leading to multiple solutions in the wind retrieval.

Within the framework of an ESA project, we try to assess the information content of spaceborne wind observations to set an objective performance measure that will allow us to not only compare different wind sensors but also seek for a future and improved sensor.

A proper determination of the Kp noise (i.e. instrument, geophysical, and GMF errors), together with the determination of generic inversion and ambiguity removal methods are crucial in order to be perform fair comparisons between the different wind sensors.

In this paper, we fully revisit the inversion problem for ERS with the aim of determining a generic inversion method for scatterometry.

2 INVERSION PROBLEM

In remote sensing, the relationship between any observation or set of observations and one or more geophysical state variables is generally represented with the following equation:

$$\mathbf{y} = K_n(\mathbf{x}) \tag{1}$$

Where $\mathbf{y}$ is the vector of observations, $\mathbf{x}$ is the vector of state variables that $\mathbf{y}$ depends on, and the operator K_n is the so-called forward model, which relates the state variables to the observations; the subscript n reminds us that it might be non-linear. The process of deriving the best estimate of $\mathbf{x}$ for a given $\mathbf{y}$, allowing for observation errors, is called inversion. In scatterometry, $\mathbf{x}$ corresponds to the sea-surface wind vector and $\mathbf{y}$ to the radar backscatter measurements (σ^o).

The most general approach used for inverting winds from scatterometer measurements is the Bayesian approach. From the Bayes' theorem, we can state that the probability of having a "true" wind given a set of backscatter measurements is proportional to the probability of having a set of backscatter measurements given the "true" wind, multiplied by the prior wind probability:

$$P(\sigma_s^o \left| \sigma_m^o \right.) = P(\sigma_m^o \left| \sigma_s^o \right.) \cdot P(\sigma_s^o) \tag{2}$$

where $\sigma_m{}^o$ is the set of backscatter measurements and $\sigma_s{}^o$ is the representation of the "true" wind in σ^o space. As such, by formulating Bayes in σ^o space (see Eq. 2), [1] interprets the prior wind probability as the a priori probability density of having a "true" set of measurements ($\sigma_s{}^o$) somewhere in the multidimensional σ^o space, i.e., $p(\sigma_s{}^o)$.

Based on Eq. 2, a common way of inversion consists of minimizing the following maximum likelihood estimator (MLE) for varying wind speed and direction ([2], [3]):

$$MLE = \frac{1}{N} \sum_{i=1}^{N} \left(\frac{\sigma_{mi}^o - \sigma_{si}^o}{Kp(\sigma_{Ni}^o)} \right)^2 \tag{3}$$

Where N is the number of measurements, $\sigma_{mi}{}^o$ is the backscatter measurement, $\sigma_{si}{}^o$ is the backscatter simulated through the Geophysical Model Function

(GMF) for different wind speed and direction trial values, and $\sigma_{Ni}{}^{o}$ is usually taken to be either $\sigma_{mi}{}^{o}$ or $\sigma_{si}{}^{o}$. Here, $Kp(\sigma_{Ni}{}^{o})$ is the observation error (noise) and has the form of Kp_i x $\sigma_{Ni}{}^{o}$, where Kp_i is a dimensionless value which is represented (for any given measurement) in the following way:

$$Kp = \sqrt{Kp_{geoph}^2 + Kp_{instr}^2} \quad (4)$$

Where Kp_{geoph} is the so-called geophysical noise, i.e. noise caused by the spatial wind variability within the resolution cell (footprint) and the non-uniform spatial averaging inherent in the radar measurement, and Kp_{instr} is the instrument noise, i.e. noise produced by the technical properties of the radar. Note that Eq. 4 should also include a GMF error term. Given many measurements, the GMF error is represented by the misfit between the measurements and the GMF. However the misfit is generally small compared to K_{geoph} and Kp_{instr} and therefore neglected in Eq. 4. [Note: strictly speaking, when assuming Gaussian errors, a term $\ln(Kp(\sigma_{Ni}^{o}))$ should be added to the right-hand side of Eq. 3 but this term is not significant and, as such, is not used].

As discussed in chapter 2 of [4], the MLE formulation (Eq. 3) is derived from the use of the Bayesian approach (Eq. 2) with the following set of assumptions: measurements are uncorrelated, their errors are Gaussian, and the a priori probability $p(\sigma_s{}^{o})$ is constant.

The approximation of constant $p(\sigma_s{}^{o})$ is problematic in scatterometry. However, for scatterometers, the use of Eq. 3 generally gives useful results in terms of wind retrieval accuracy. This is not the case for the retrieved wind direction, which skill is somehow degraded (see [1] for ERS, and [4] for Seawinds).

2.1 Wind direction skill

For a given scatterometer, its set of N σ^{o} measurements defines a GMF surface in a N-dimensional σ^{o} space for varying speed and direction. For the ERS triplet $(\sigma_1{}^{o},\sigma_2{}^{o},\sigma_3{}^{o})$, this surface has the shape of a cone in the 3D space (see chapter II of [1]).

Reference [5] investigated the effect of normalization in Eq. 3 through visualization of differently scaled 3D measurement spaces. Fig. 1a shows a section of the cone in which the backscatter measurements (triplets) are scaled by a constant Kp value and Fig. 1b shows the same cut without scaling and in a transformed space where the axes are $z_i = (\sigma_i^{o})^{0.625}$.

Reference [5] show that to be able to obtain both accurate wind directions and a realistic wind direction probability density after inversion, it is desirable that equal portions of the σ^{o} triplets are thrown onto equal wind direction intervals. This is the case if the GMF surface has no sharp curvature and is circular (Fig. 1b) rather than elliptic (Fig. 1a). [Note: A circular shape of the cone for a uniform wind direction probability density is equivalent to a constant $p(\sigma_s{}^{o})$].

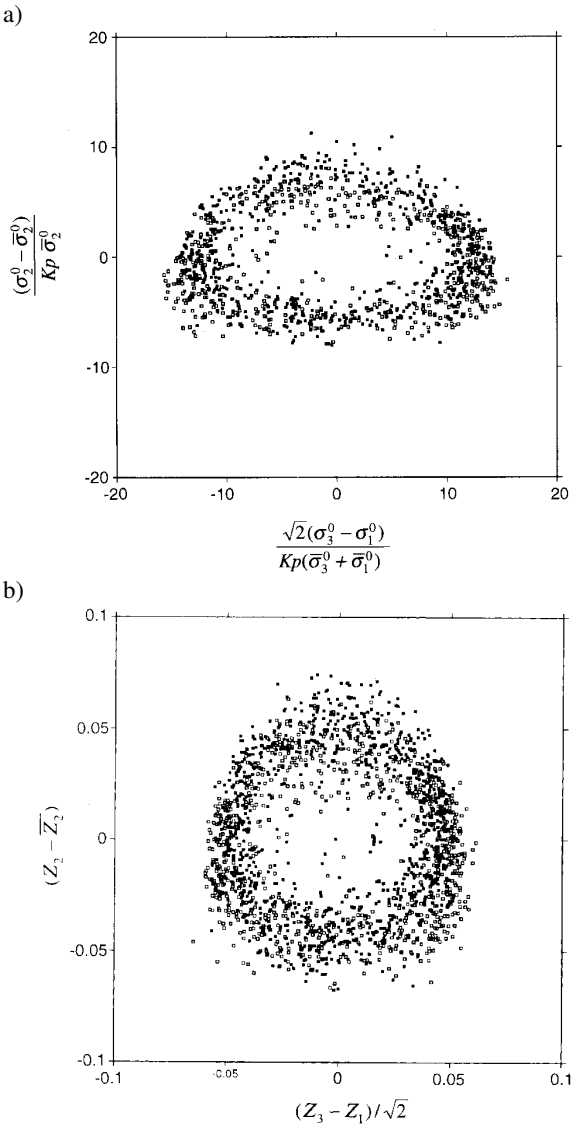

Fig. 1. Intersection of the cone with the plane $\sigma^{o}_1 + \sigma^{o}_3 = 2\sigma^{o}_{ref}$, with a thickness of $0.05\sigma^{o}_{ref}$ for node 7, for values of σ^{o}_{ref} corresponding approximately to a speed of 8 m/s. In (a) σ^{o}_1, σ^{o}_2, and σ^{o}_3 values are scaled by Kp, equal to 0.05, and in (b) the cut is made in a transformed space where the axis are $z_i = (\sigma_i^{o})^{0.625}$.

As such, when the cone is elliptic, certain wind directions are favoured in the retrieval process, leading to artificial accumulations in the retrieved wind direction distribution (see [5]). [Note that the same effect is seen for Seawinds when using Kp normalization in Eq. 3 ([4])].

Consequently, by transforming the measurement space and removing the Kp noise normalization from Eq. 3, the assumption of constant $p(\sigma_s^o)$ becomes practicable (i.e., the cone is circular) and the wind direction retrieval is improved. In other words, for ERS inversion, the shape of the solution surface (i.e., cone shape) is more important than the information on the noise (i.e., Kp normalization).

However, [5] used only instrument noise (a constant value of 0.05) in the measurement noise (Eq. 4) to show that $p(\sigma_s^o)$ is far from constant. No attempt was done at that time to test the geophysical noise model for ERS wind retrieval. Therefore, we first analyse in detail the noise properties of the system and check whether the inclusion of a more realistic *Kp* in Eq. 3 makes the assumption of constant $p(\sigma_s^o)$ valid for ERS and therefore validates Eq. 3 as a generic inversion method.

3 IMPACT OF A REALISTIC NOISE IN INVERSION

3.1 Determination of geophysical noise parameters

As mentioned before, we presume that the geophysical noise is caused by the sub-footprint spatial wind variability and the non-uniform spatial sampling of backscatter measurements. In particular, for ERS, several sub-cell resolution σ^o measurements are averaged to produce a single σ^o measurement for every beam (i.e., fore, mid, and aft). These sub-cells are centered in different locations of the footprint and as such observe somewhat different winds due to wind variability. Therefore, the geophysical noise will depend on both the sub-footprint wind variability and the number of independent σ^o samples. [Note: both the number of independent samples and the wind variability are determined by the sub-cell resolution].

In order to derive the geophysical noise, a simulation of the backscatter triplets (fore, mid, aft) is performed and compared to real triplets. In the simulation, we assume as input a true wind Gaussian distribution centered at 0 m/s with a standard deviation (SD) of 6 m/s in the wind components. Then, for each input wind vector we simulate the triplets using the CMOD-5 GMF ([6]) for different values of wind variability and σ^o samples. [Note: a constant instrument noise (Kp_{instr}) value of 0.05 ([5]) is used in the simulation].

Fig. 2 shows the real and simulated triplets that belong to a particular section of the cone (for analysis purposes, the section has a certain thickness in order to allow a significant amount of triplets in the plot). Both CMOD-4 ([7]) and CMOD-5 GMF cone sections are also shown. The uppermost triplets correspond to winds blowing along the mid beam (upwind/downwind), whereas at the lowest points the wind blows roughly across the mid beam (crosswind).

a)

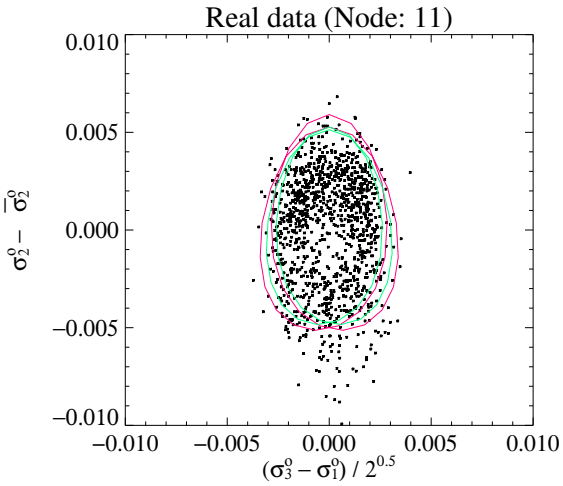

b)

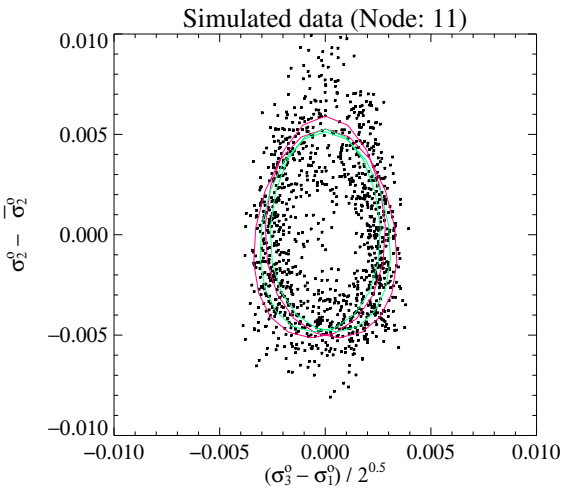

Fig. 2. Same as Fig. 1 but in non-scaled measurement space, for node 11 and a wind speed of 4.3 m/s. (a) shows the real triplet distribution and (b) the simulated data assuming 0.75 m/s variability and 8 σ^o samples. The curves for both CMOD-4 (red) and CMOD-5 (green) are plotted.

Fig. 2a shows that most of the real triplets are located in the inner side of both CMOD-4 and CMOD-5 sections. This is a clear sign that the GMF sections are too big at low winds (the cone section in this Figure corresponds to winds around 4.3 m/s). Note that the simulated triplets (Fig. 2b), which are derived using CMOD-5, are distributed at either sides of CMOD-5 sections (green line), further confirming the GMF misfit at low winds. It is also discernible from Fig. 2a that, although CMOD-5 shows some misfit, the latter better fits the real data than CMOD-4.

Taking into account the effect of using an imperfect GMF in the simulation (i.e., section expansion of triplet distribution), Fig 2b is the simulation, which resembles best the real data (Fig. 2a). The rest of the simulations, corresponding to different wind variability (0.5-1 m/s) and sampling number (5-8) assumptions, show either too much or too little noise (not shown). Fig. 2b corresponds to a wind variability of 0.75 m/s and 8 σ^o samples. Therefore, from now on, we will use these parameters for further simulations.

Looking at the excess of noise at the top of the simulated triplet distributions (Fig. 2b), one could conclude that the upwind/downwind region of CMOD-5 is too high. However, more research is required in order to consistently correct the mentioned misfit at the associated wind speed and incidence angle.

Again, taking into account the impact of such misfit in our plots, there is a good agreement between real and simulated triplets. As such, we can conclude that the selected geophysical noise parameters are realistic. Moreover, at higher wind speed cone sections (e.g., 8 m/s), where the CMOD-5 GMF shows no misfit problem, there is a very good agreement between the real and simulated data (not shown), further validating our parameter selection.

3.2 Derivation of a geophysical noise model

In order to derive a geophysical noise model, we study the impact of the derived geophysical noise parameters (see section 3.1) on the mean σ^o value and its uncertainty (SD) in terms of dependencies on wind speed, wind direction, and incidence angle. This sensitivity study is performed over a wide range of wind speeds [0-20 m/s], wind directions [0°-360°], and incidence angles [16°-66°]. Thus, for any given "true" σ^o (corresponding to an input or "true" wind speed, wind direction and incidence angle within the mentioned ranges), a distribution of σ^o corresponding to a wind (component) variability of 0.75 m/s over the "true" wind is generated. The SD of the distribution is computed and reduced by a factor of $1/\sqrt{8}$ due to the noise level reduction in the averaging process (i.e., as determined in section 3.1, a total of 8 sub-cell σ^o samples are averaged for every ERS beam).

The mean of the σ^o distribution shows no significant difference compared to the "true" σ^o as a function of wind speed or incidence angle (not shown). However, there are some significant differences (biases) as a function of wind direction, especially for high incidence angles and low winds (not shown), denoting that the wind direction sensitivities play an important role in inversion.

However, these biases are corrected in the GMF by definition. That is, the GMF is a fit of the mean of the σ^o distribution to some reference ("true") winds. As such, the deviations of the mean σ^o from the "true" σ^o are taken into account in the GMF fit. Therefore, these biases are not expected to have any significant impact on the quality of wind retrieval. The uncertainty in the mean however would certainly have an effect.

The SD of the σ^o distribution represents uncertainty in terms of geophysical noise. Dependencies on wind speed and incidence angle are clearly discernible (see shape of Fig. 3). Dependencies on wind direction are also discernible (not shown). However, the inclusion of the wind direction dependency in the noise model could have a negative impact on wind retrieval. As discussed in [8], the shape of the GMF surface makes certain wind directions to be favoured and therefore systematically assigned in the inversion. Including wind direction dependencies in the MLE (e.g., setting a wind direction dependent *Kp*) will most likely make such inversion problem more acute. As such, we compute a geophysical noise model dependent on wind speed and incidence angle only.

To neglect the wind direction dependency, we average the geophysical noise over all wind directions. Fig. 3 shows the average geophysical noise surface (Kp_{geoph}) as a function of wind speed and incidence angle. Given a constant Kp_{instr} of 5% ([5]), the total *Kp* can be easily derived using Eq. 4.

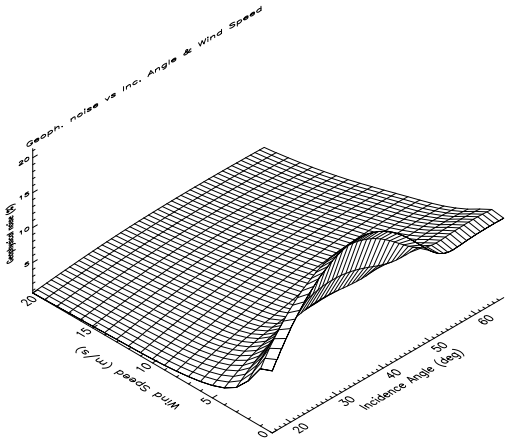

Fig. 3. Average geophysical noise as a function of wind speed and incidence angle. The speed binning is 1 m/s and the angle binning is 1°.

In order to show the error in the estimation of Kp_{geoph} produced by neglecting the wind direction dependency, we examine the discrepancies between the average geophysical noise and the geophysical noise corresponding to a wind direction of 0°. The discrepancy is maximal at high incidence angles for high and very low wind speeds. However, taking into

account the 5% instrument noise, the impact of such discrepancies (up to 1.5%) in the total *Kp* is negligible.

3.3 Impact of derived Kp in inversion

As discussed in section 2, in order to retrieve accurate winds for ERS, it is important to make practicable the assumption of constant $p(\sigma_s^o)$, i.e., the cone circular.

Fig. 4 shows the same cone section as for Fig. 1 in which the backscatter measurements are scaled by the realistic *Kp* derived in section 3.2. The cone section in Fig. 4 is rather elliptic and very similar to the cone section with fixed *Kp* scaling (Fig. 1a). Note that Fig. 4 is far from the circular shape shown when measurement space is transformed into z space (Fig 1b). Similar results are derived when comparing cone sections at different wind speed cuts and WVC numbers.

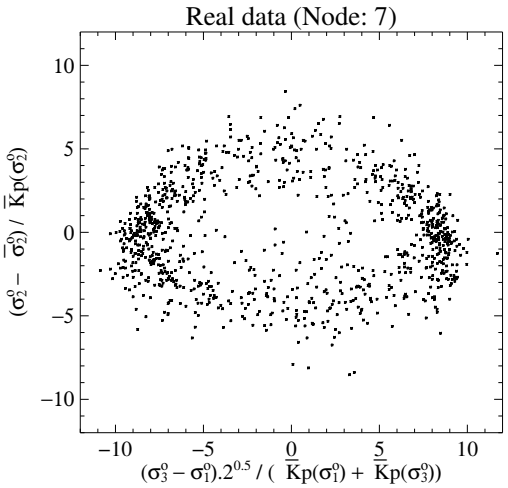

Fig. 4. Same as Fig. 1b but for triplet values scaled by the derived *Kp*.

Therefore, despite the use of a good measurement noise model in the MLE normalisation (Eq. 3), the wind direction accuracy is not satisfactory since $p(\sigma_s^o)$ is far from being locally constant (see discussion in section 2.1). In other words, we can eventually conclude that the shape of the cone is more important than the noise properties of the system for inversion.

4 GENERIC INVERSION METHOD

According to the results presented in section 3, a space transformation, which makes true the assumption of constant $p(\sigma_s^o)$, i.e., z space, is desirable for ERS. Since the aim of this work is to set a generic method for scatterometer wind retrieval, we should now try to determine the corresponding space transformation for NSCAT or QuikSCAT. However, this is not straightforward. In contrast with ERS, where the transformation could be analytically derived since the measurement space is 3-dimensional, NSCAT and QuikSCAT measurement systems are 4-dimensional.

We therefore propose to set a generic method that seeks for the best measurement space transformation in a numerical way. The method is based on the scaling or calibration of the different scatterometer beams. Since the optimal transformation is already known for ERS (i.e., z space), we use the latter to validate the proposed method.

4.1 Calibration method

In order to look for an interesting property of circularity, which can be generically used by all scatterometers, let's first look at the 2-dimensional case.

A circle is defined by a set of two functions, which depend on an angle ϕ in the following way:

$$x = r \cdot \cos\phi \; ; \; y = r \cdot \sin\phi \tag{5}$$

where *x* and *y* represent the horizontal and vertical axis, respectively, and *r* is the radius of the circle and therefore a constant value. From Eq. 5, it can be easily derived the following expression of the total sensitivity:

$$\left\| \frac{\partial \vec{x}}{\partial \phi} \right\| = \left(\frac{\partial x}{\partial \phi} \right)^2 + \left(\frac{\partial y}{\partial \phi} \right)^2 = \text{constant} \tag{6}$$

That is, the total sensitivity to direction changes remains constant for any value of ϕ, ranging from 0° to 360°. Or, in other words, the distance $\vec{x}$ travelled for a small change in ϕ is the same for all ϕ.

Similarly, such constant-distance property can be applied in scatterometry to any N-dimensional measurement system. As such, constant-distance is true when a set of functions, i.e., σ° beams, which depend on an angle ϕ, i.e., wind direction, follow the expression:

$$\left\| \frac{\partial \overrightarrow{\sigma^o}}{\partial \phi} \right\| = \sum_{i=1}^{N} \left(\frac{\partial \sigma_i^o}{\partial \phi} \right)^2 = \text{constant} \tag{7}$$

where N=3 for ERS, and N=4 for NSCAT or SeaWinds. Therefore, in order to obtain circularity, we must make Eq. 7 as true (i.e., constant) as possible. That is, when Eq. 7 is not true, we must find a transformation of $\overrightarrow{\sigma^o}$, i.e., $\overrightarrow{\sigma'}$, which satisfies the following:

$$\left\| \frac{\partial \overrightarrow{\sigma'}}{\partial \phi} \right\| \approx \text{constant} \tag{8}$$

Minimization

The left plots of Fig. 5 represent the total sensitivity (solid curves) of CMOD-5 GMF as a function of wind direction for a few WVC numbers and wind speed

values. The dotted, dashed, and dash-dotted curves represent the individual fore-, mid- and aft-beam sensitivities, respectively, which contribute to the total sensitivity (see Eq. 7). The straight line corresponds to the mean total sensitivity over all wind directions:

$$Mean = \frac{1}{M}\sum_{j=1}^{M}\sum_{i=1}^{3}\left(\left.\frac{\partial\sigma_i^o}{\partial\phi}\right|_{\phi_j}\right)^2 \quad (9)$$

where M is the number of wind direction intervals, i.e., 360 in this case.

In line with the results shown in section 3.3, these plots also show that using Kp normalization in the MLE inversion (see Eq. 3) makes the cone far from being circular (note that the solid curves are far from being straight lines).

The goal of the method that we propose is to flatten as much as possible the mentioned (solid) curves. In order to do so, we scale the individual beam sensitivities such that the resulting total sensitivity is closest to its mean value. In other words, we minimize the distance between the solid curve (total sensitivity) and the straight line (mean value) by re-scaling the dotted, dashed and dash-dotted lines (individual beam sensitivities). As such, the cost function we want to minimize looks as follows:

$$J = \frac{1}{M}\sum_{j=1}^{M}\left[\sum_{i=1}^{3}\left(a_i\cdot\left.\frac{\partial\sigma_i^o}{\partial\phi}\right|_{\phi_j}\right)^2 - Mean\right]^2 \quad (10)$$

where J is the cost function and a_i the scaling or calibration coefficients. Note that since $a_i \neq a_i(\phi)$, the minimization is analogous to looking for a transformation (scaling) $\overrightarrow{\sigma'} = \vec{a}\cdot\overrightarrow{\sigma^o}$, which obeys Eq. 8.

Also note that we have chosen the squared distance (between total sensitivity and the mean) rather than the distance (see Eq. 10) for minimization since the results (not shown) reveal that the former is more effective than the latter in flattening the total sensitivity curve.

For every wind speed and WVC number, J is minimized and a set of a_i found. The minimization results in a clear single minimum (for every wind speed and WVC number), indicating that the method is robust and un-ambiguous. For more detailed information on the a_i coefficients, see [9].

The left plots from Fig. 5 show the sensitivity in σ^o space (from here on referred to as "Kp norm", since it uses the derived Kp normalization in the MLE inversion) and the right plots show the sensitivity in σ' space, i.e., after calibration (from here on referred to as "calibrated Kp norm"). By comparing either sides of Fig. 5, one can easily see that, in general, the calibration is effective in flattening the total sensitivity curve, i.e. making the cone more circular. The calibration is most effective for low and mid winds at the inner swath (WVC numbers 1-6) region (see top and mid plots). However, it is little effective for high winds and the outer swath (WVC numbers 13-19) region (see bottom plots). In this case, the individual beam sensitivities (see Fig. 5e) contribute in a similar way to the total sensitivity (in contrast with Figs. 5a and 5c, where fore and aft beams especially contribute to the peaks while the mid beam contributes to the troughs), and therefore scaling does not help much in flattening the total sensitivity curve.

Another interesting result is that the mean total sensitivity remains almost the same after calibration (compare straight lines at either sides of Fig. 5), denoting consistency in the calibration procedure. More results on the calibration skill are shown in Fig. 6

Fig. 6 shows the histograms of the gradient[1] of the total sensitivity curves from Fig. 5. The dotted lines correspond to histograms of Kp norm and the solid lines to histograms calibrated Kp norm. The distribution of gradients shows how flat the total sensitivity curve is, i.e., the lower the gradients are, the flatter the total sensitivity curve. Figs 6a and 6b show a much narrower gradient distribution around zero after calibration (see difference between solid and dotted distributions), denoting the good skill of the calibration procedure for low/mid wind speeds and inner swath region. Fig. 6c shows almost no difference in the distributions before and after calibration, denoting the reduced effectiveness of the procedure for high winds and the outer swath.

4.2 Validation

In this validation, we mainly show results in terms of wind direction skill since the calibration procedure is expected to improve this component most. Moreover, the results (not shown) reveal no significant wind speed skill difference between the three inversion types tested here, i.e., z space, Kp norm and calibrated Kp norm.

The schemes which approach a circular cone, i.e., z space and calibrated Kp norm, are expected to perform better than the Kp norm scheme where the latter shows less circularity (more ellipticity), i.e., in the inner swath (see [9]). The results indeed show better agreement with ECMWF, in terms of wind direction retrieval, for

[1] The noise of the total sensitivity curves in Fig. 5 is filtered out by an averaging procedure to produce the results shown in Fig. 6. This noise is a numerical artefact produced by the different wind direction sampling between the curves (1°) and the CMOD-5 look-up-table (2.5°) and, as such, has no geophysical meaning.

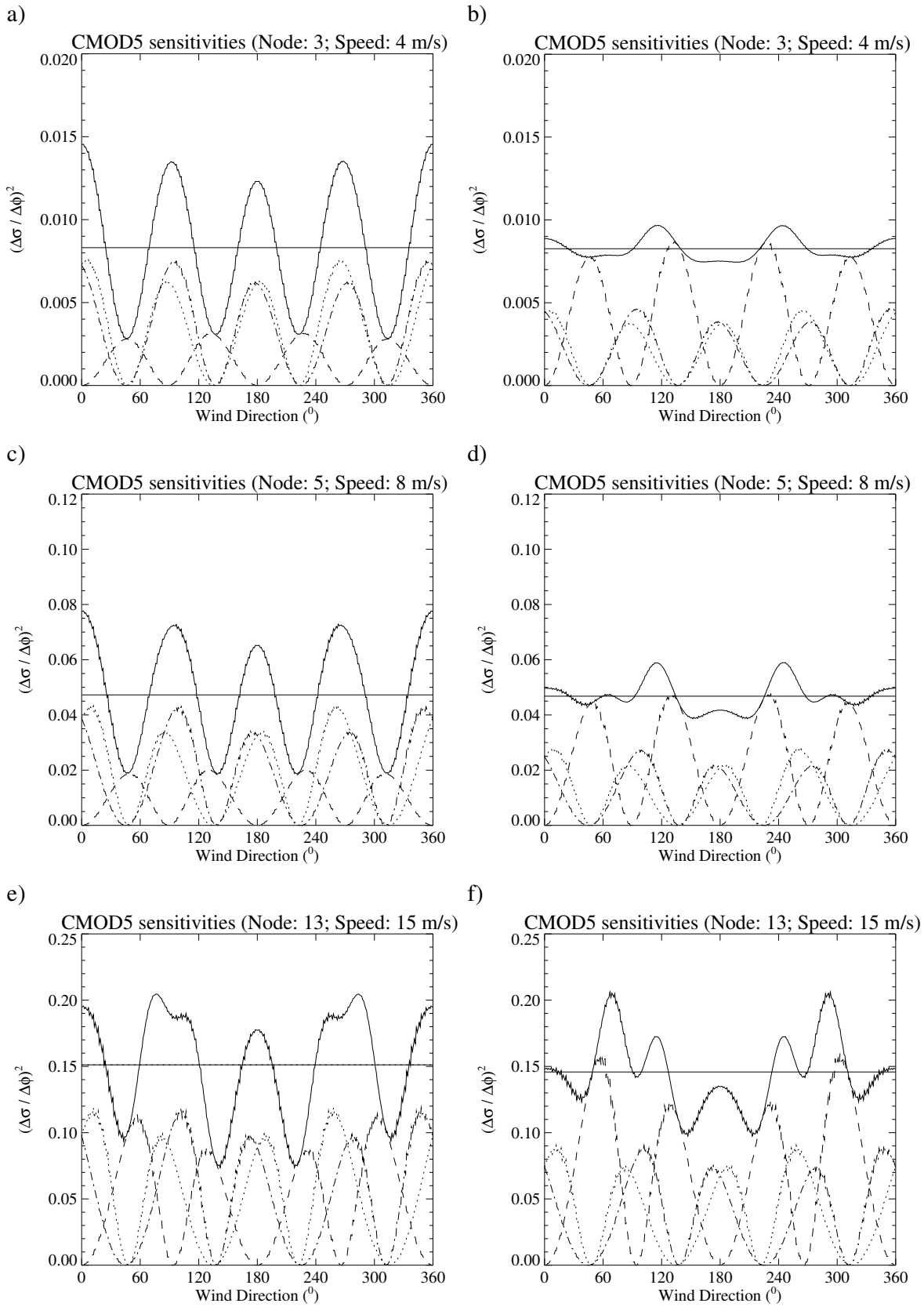

Fig. 5. CMOD-5 total sensitivity (solid curves) as a function of wind direction for Kp norm (left plots) and calibrated Kp norm (right plots) for a few WVC numbers and wind speed values: node 3 and 5 m/s (top plots), node 5 and 8 m/s (mid plots), and node 13 and 15 m/s (bottom plots). The dotted, dashed, and dash-dotted curves represent the individual fore-, mid- and aft-beam sensitivities, respectively. The straight line corresponds to the mean total sensitivity over all wind directions.

z space and calibrated Kp norm than for Kp norm inversion, especially at the inner swath region (not shown).

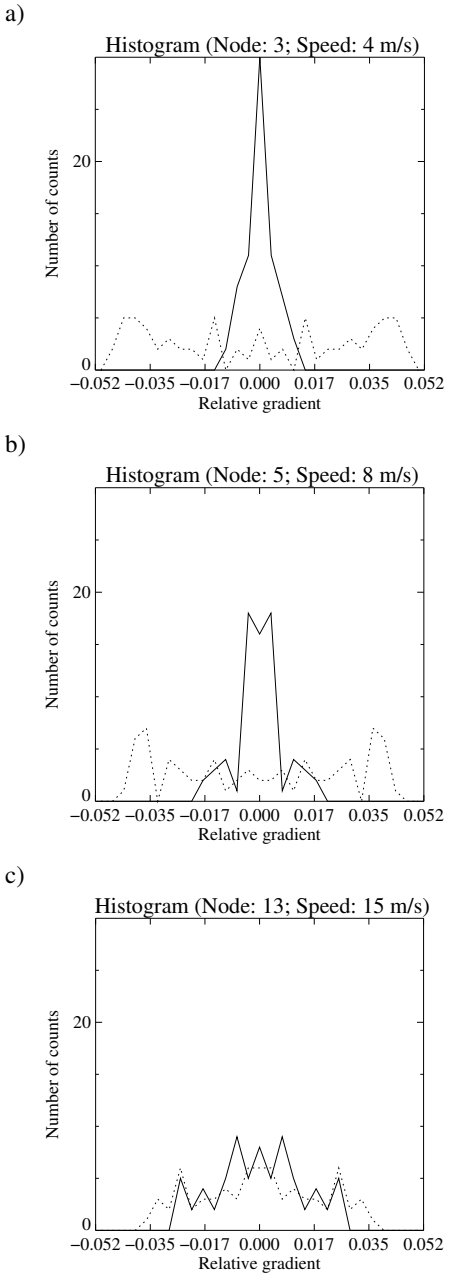

Fig. 6. Histograms of the gradients of the total sensitivity curves from Fig. 5 for a few WVC numbers and wind speed values: (a) node 3 and 5 m/s, (b) node 5 and 8 m/s, and (c) node 13 and 15 m/s. The gradient values are relative to the mean total sensitivity. The dotted lines correspond to histograms of Kp norm and the dotted lines to histograms of calibrated Kp norm.

As mentioned in section 2, the shape of the cone plays a crucial role in the wind direction retrieval. As the cone becomes more elliptic (less symmetric), certain directions are favoured in the retrieval process, causing in turn some artificial accumulations in the retrieved wind direction distributions. This systematic effect becomes more acute for points lying far away from the cone surface, i.e., for triplets with high MLE values.

Fig. 7 shows the wind direction distributions for triplets with MLE larger than 0.7 (note that triplets with MLE larger than 9 are screened out). Looking at the left plots, some systematic accumulations at certain wind directions are discernible in the ERS-retrieved distributions (dotted) with respect to the ECMWF distributions (solid). These accumulations are largest for Kp norm inversion (Fig. 7c) and smallest for z space (Fig. 7a). The calibration (Fig. 7e) reduces the problem with respect to the Kp norm inversion, although it is not as effective as the z-space transformation.

However, if we look at the inner swath distributions (right plots), the region in which the calibration is optimal (see section 4.1), it is clear that the calibrated Kp norm distribution (Fig. 7f) is very similar to the z space one (Fig. 7b), and much improved with respect to the Kp norm distribution (compare peaks at 0° and 180° in Figs. 6d and 6f). Note that although these triplets have high MLE values, they are still of reasonable quality (see reasonable agreement between ECMWF and ERS-retrieved distributions from top and bottom plots) and therefore very important to keep since they represent about 4% of the total amount of the ERS wind observations.

Finally, we have also looked at the ERS inversion problem for low winds (not shown). The results show no significant differences between the three inversion types, which show substantial wind direction errors. The reason for this is that the backscatter noise for low winds is very high as compared to the size of the cone, leading to systematic errors in the wind direction assignment (accumulations in the wind direction distributions).

In summary, we conclude that although z space is the optimal transformation for ERS in terms of the wind direction retrieval, the proposed calibration method represents an improvement with respect to Kp norm and therefore an alternative to z space. In contrast to z space, the calibration method is generic and can be applied to any scatterometer system.

5 CONCLUSIONS

In this paper, we revisit the inversion procedure for ERS in order to set a generic inversion for scatterometers.

In contrast with NSCAT and Seawinds, ERS uses no *Kp* normalization in the MLE inversion to optimize wind

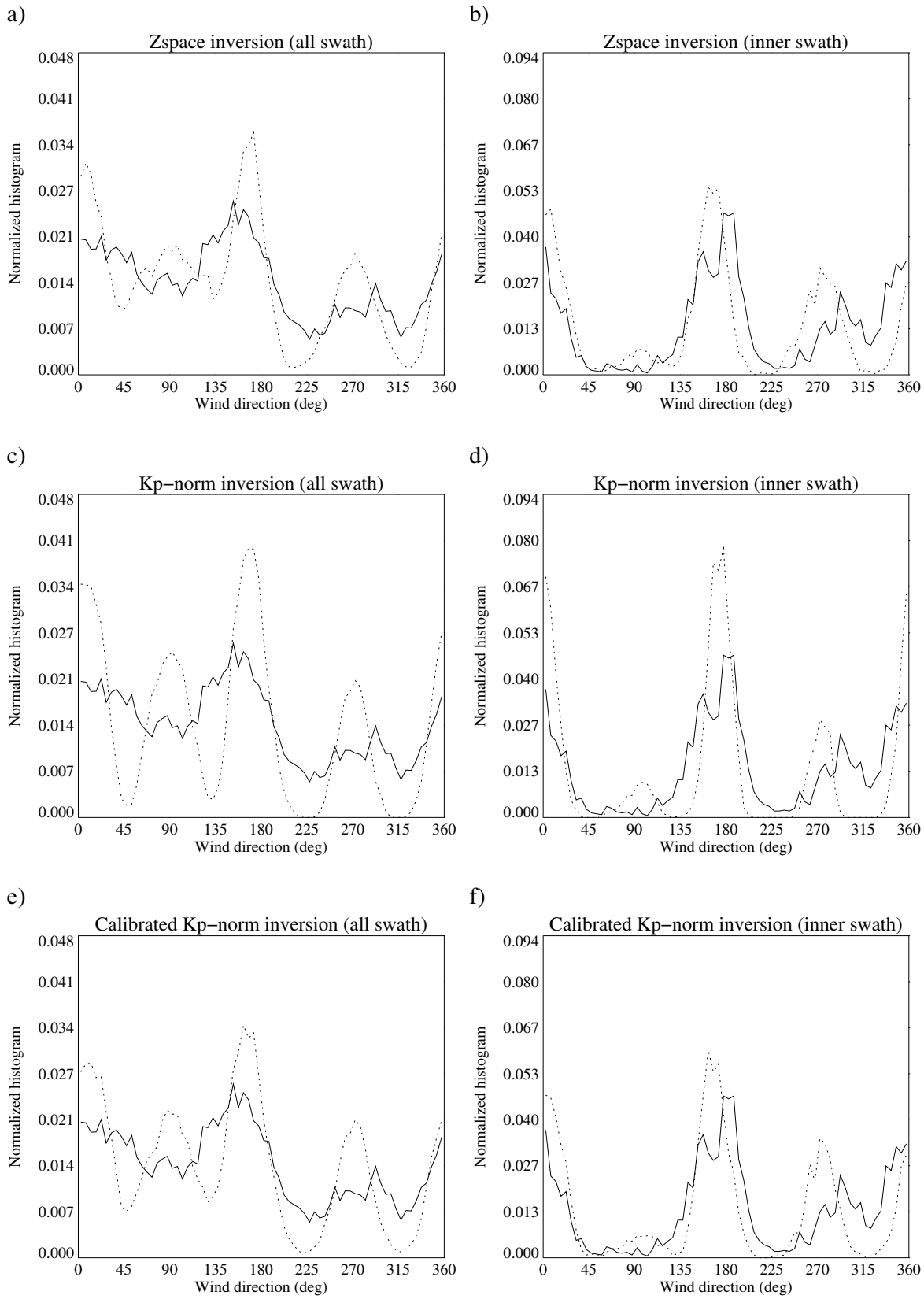

Fig. 7. Wind direction (with respect to the satellite flight direction) distribution of the ERS-retrieved solution closest to ECMWF (dotted) for z space (top), Kp norm (mid), and calibrated Kp norm (bottom) and for the inner swath (right) and the entire swath (left). The solid line corresponds to the ECMWF wind direction distribution. The distributions only contain triplets with MLE larger than 0.7. The direction binning is 5°.

retrieval. Reference [5] show that by using no Kp normalisation in the MLE inversion and by transforming the measurement space (i.e., z space), the cone shape becomes circular and the wind retrieval improves. As a first attempt to find a generic inversion method that is suitable for all scatterometer systems, the *Kp* normalization is re-visited for ERS, this time including geophysical noise information.

Through visualization of the 3D measurement space, real triplets are compared to simulated triplets for different geophysical noise parameter values. Then, the parameters that better represent the real triplet distributions are selected and used for computing the geophysical noise model. The simulations well reproduce the real data and, as such, validate the derived geophysical noise model for different WVC numbers and wind speeds.

Despite the successful derivation of the geophysical noise, the *Kp* normalization produces unsatisfactory results in terms of MLE inversion, i.e. the resulting cone shape becomes rather elliptic thus reducing the wind direction retrieval quality. We therefore conclude that the shape of the cone is more important than the noise properties for inversion.

A generic method that seeks for the best measurement space transformation in a numerical way is presented. The method is based on the calibration of the different beam sensitivities.

The calibration procedure is most effective, in terms of producing a more circular cone, at the inner swath (WVC numbers 1 to 6), especially for low and mid winds, and least effective for high winds and outer regions (WVC numbers 13 to 19).

We validate the calibration against ECMWF winds, using as a reference the z space and the non-calibrated (Kp norm) inversions. The main differences between the inversions lie in the wind direction domain. Although the highest wind direction skill corresponds to the z-space inversion, the calibration shows improvement with respect to Kp norm, especially in the inner swath where its skill is similar to the z space skill.

As such, the calibration method turns out to be a good alternative to the z-space inversion, and since it is generic for scatterometer systems, we now plan to test it for Seawinds.

ACKNOWLEDGMENTS

This work is funded by the European Space Agency under the project contract number 18041/04/NL/AR. We acknowledge the help and collaboration of our project partner at IFARS, Volkmar Wismann.

REFERENCES

1. Stoffelen, A., "Scatterometry," *PhD thesis at the University of Utrecht,* ISBN 90-393-1708-9, 1998.

2. Graham, R. et al., Evaluation of ERS-1 wind extraction and ambiguity removal algorithms: meteorological and statistical evaluation," *ECMWF report*, ECMWF, Reading, United Kingdom, 1989.

3. JPL, "QuikSCAT science data product user's manual," version 2.2, *Jet Propulsion Laboratory D-12985*, pp. 89, December 2001.

4. Portabella M., "Wind field retrieval from satellite radar systems," *PhD thesis at the University of Barcelona,* ISBN 90-6464-499-3, 2002.

5. Stoffelen A. and Anderson D., "Scatterometer data interpretation: measurement space and inversion," *J. Atm. and Ocean. Techn*., vol. 14(6), 1298-1313, 1997a.

6. Hersbach H., "CMOD-5: an improved geophysical model function for ERS C-band scatterometry," *Technical Memorandum,* no. 395, ECMWF, Reading, United Kingdom, 2003.

7. Stoffelen A. and Anderson D., "Scatterometer data interpretation: derivation of the transfer function CMOD-4," *J. Geophys. Res.*, vol. 102(C3), 5767-5780, 1997b.

8. Portabella M. and Stoffelen A., "Rain detection and quality control of SeaWinds," *J. Atm. and Ocean Techn.*, vol. 18, no. 7, 1171-1183, 2001.

9. Portabella M. and Stoffelen A., "Study of an objective performance measure for spaceborne wind sensors," ESTEC contract, no. 18041/04/NL/AR, Netherlands.